ChemistrySelect

Research Article
doi.org/10.1002/slct.202402774

Chemistry Europe
European Chemical Societies Publishing

www.chemistryselect.org

Structure, Property, and Functionality of 2D ZnO Microplatelets with Low Photocatalytic Activity for Application as UV Filters in Sunscreens for Photoprotection

Nazia H. Kera,[a, b] Sreejarani Kesavan Pillai,[a] and Suprakas Sinha Ray*[a, b]

This study focuses on the synthesis and characterization of 2D polygonic ZnO microplatelets for application as UV filters in sunscreens. ZnO microplatelets are obtained via a simple method involving chemical precipitation, aging, and calcination. XRD, SEM, and TEM analyses confirm the successful formation of ZnO microplatelets. DRUV-Vis studies indicate that the ZnO microplatelets have a band gap energy value of 3.2 eV and exhibit good UV radiation absorption, similar to a commercial ZnO reference sample. Furthermore, in methylene blue photodegradation studies, the ZnO microplatelets show significantly lower photocatalytic activity than the ZnO reference sample. Under UV irradiation of 254 nm and 365 nm wavelengths, the dye in contact with ZnO microplatelets is photodegraded by only 38 % and 69 % after 5 h, compared to the reference sample, which photodegraded the dye by 87 % and 97 %, respectively. The performance of a sunscreen formulation containing the ZnO microplatelets (at 10 wt %), in terms of the photoprotection factors and photostability, is on par with that of a formulation containing the ZnO reference sample. Due to their microplatelet structure, good UVR absorption capacity, and relatively lower photocatalytic activity, the ZnO microplatelets show potential for application as UV filters in sunscreen products.

1. Introduction

The dangers of overexposure to ultraviolet radiation (UVR) to human health are well established.[1–3] The use of sunscreen products incorporating active UV filters (UFs) has been identified as essential for human photoprotection from UVR to prevent skin damage, disorders, and diseases. Both organic and inorganic UFs have been widely used in sunscreen products.[1–3] However, organic UFs often degrade on UV-light exposure, reducing sunscreen efficacy and generating harmful reactive species that may cause skin irritation, allergies, and sensitization. Inorganic UFs such as ZnO and TiO_2 are favored over organic UFs for sunscreen products due to their high photostability and capacity for broad-spectrum UV protection.[1] Currently, ZnO and TiO_2 are the only two inorganic UFs approved by regulatory bodies such as the United States Food and Drug Administration (USFDA).[1,2] Microsized particles of TiO_2 (150–300 nm) and ZnO (200–400 nm) have been widely used in sunscreen products in the past few decades and offered effective photoprotection of skin.[2] However, when applied on the skin, these sunscreen products show an aesthetically undesirable white residue due to the scattering of visible light due to the relatively large sizes and high refractive indices of the ZnO and TiO_2 microparticles.[1–3] Obtaining stable sunscreen formulations is also technically difficult when incorporating microsized ZnO and TiO_2 particles, which can destabilize the emulsions.[4] To overcome these unfavorable effects, ZnO and TiO_2 microparticles in sunscreen products have largely been replaced by NPs, which reflect significantly less visible light than microparticles and appear transparent when applied to the skin.[1–3] TiO_2 particles of sizes 10–20 nm and ZnO particles of sizes 200 nm or below appear transparent in sunscreen applied on the skin.[5] However, a major disadvantage of the reduction of particle size is the associated increase in the band gaps of both TiO_2 and ZnO, which shifts the UV-visible absorption spectrum of these inorganic UFs away from the UVA region and towards the UVB region, thus compromising UVA absorption and broad-spectrum photoprotection.[2,5] Another disadvantage is the aggregation of NPs, an inherent tendency due to their relatively high interfacial energies that may reduce their transparency, the efficacy of sunscreen products, and the formulation stability over time.[4,5] The photoreactivity of ZnO and TiO_2 NPs due to their semiconducting nature has raised concerns over the safety of their use in sunscreen products.[1–3] Due to their photocatalytic ability, the absorption of UVR by ZnO and TiO_2 NPs generates free radicals and reactive oxygen species (ROS), which may cause damage to the skin through potential genotoxic and cytotoxic effects.[1–3] The generated free radicals could also degrade organic compounds in the sunscreen formulation, causing discoloration and reducing product stability.[6,7] Due to their diminutive size, there are concerns regarding the dermal penetration of TiO_2 and ZnO

[a] N. H. Kera, S. K. Pillai, S. S. Ray
Centre for Nanostructured and Advanced Materials, DSI-CSIR Nanotechnology Innovation Centre, Council for Scientific and Industrial Research, Pretoria 0001, South Africa
E-mail: rsuprakas@csir.co.za

[b] N. H. Kera, S. S. Ray
Department of Chemical Sciences, University of Johannesburg, Doornfontein Johannesburg 2028, South Africa

Supporting information for this article is available on the WWW under https://doi.org/10.1002/slct.202402774

NPs from sunscreen products and the potential toxic effects of these NPs in the human body and to organisms in the environment.[1–3] Different methods have been investigated to mitigate the disadvantages of using NPs in sunscreen products while maintaining high UVR attenuation capacity.[1–3] One method employed has been coating NPs with different substances such as silica, methicone, aluminium hydroxide, aluminium oxide, polymethylacrylic acid or biopolymers.[1–3] However, these coatings often do not completely diminish the photocatalytic effects of ZnO and TiO_2 NPs and have variable durability under UV irradiation.[1,5] The use of hierarchical structured composite UFs, obtained through the controlled agglomeration of ZnO and/or TiO_2 NPs and microparticles, is a promising method investigated for circumventing the use of NPs as UFs while retaining their desirable properties.[6,8] Reinosa et al.[8] used a dry dispersion method to obtain a ZnO-TiO_2 composite comprising TiO_2 NPs (~15 wt.%) anchored onto ZnO microparticles (~85 wt.%). The ZnO–TiO_2 composite had a broader UVR absorbance range than the TiO_2 NPs and ZnO microparticles individually. A sunscreen formulation containing the prepared composite at 10 wt% had a higher SPF value of 9.1 than a formulation containing a combination of TiO_2 NPs and ZnO microparticles, with an SPF value of 5.7. The higher SPF value obtained for the composite was attributed to a synergistic effect between the ZnO microparticles and the anchored TiO_2 NPs, while the SPF obtained for the TiO_2 NP/ZnO microparticle combination was due to an additive effect. Reinosa et al.[6] later prepared a ZnO-TiO_2 composite in which ZnO NPs were deposited onto TiO_2 microparticles via a sol-gel method. The UV absorption maximum and band gap energy of the composite were found to be between that of ZnO NPs and TiO_2 microparticles. A sunscreen formulation containing the ZnO-TiO_2 composite had a slightly higher SPF value attributed to light scattering by the anchored ZnO NPs. It exhibited higher photostability than a formulation containing TiO_2 microparticles due to the hierarchical structure of the composite, which partially inhibited the generation and propagation of ROS and free radicals. These studies corroborated that the structural properties of ZnO and TiO_2 particles, such as their shape, size, and thickness, greatly influence their UVR shielding and photocatalytic properties and can be tailored towards their application as UFs in sunscreen products.

Two-dimensional (2D) ZnO nanomaterials have recently been investigated for various applications, including catalysis, electronics, gas sensing, and adsorption, due to their unique properties, such as high surface area-to-volume ratios and high specific surface areas.[9,10] This study focuses on the synthesis and characterization of 2D polygonic ZnO microplatelets for application as UFs in sunscreen products. It is proposed that the 2D structure of the ZnO microplatelets, comprising thin plates with a high surface area-to-volume ratio, will be effective for facilitating effective UVR attenuation through absorption, scattering, and reflection mechanisms. Due to their size and structure obtained through the controlled agglomeration of NPs, the 2D polygonic ZnO microplatelets are also expected to have lower photoactivity than corresponding NPs and commercial ZnO microparticles. As a result, sunscreen formulations containing the 2D polygonic ZnO microplatelets are expected to have higher photostability than those containing NPs and commercial ZnO particles. The risk of 2D polygonic ZnO microplatelets in sunscreens penetrating the skin and causing toxic effects in the body is also substantially lower than the risk associated with using sunscreens incorporating ZnO NPs. Furthermore, the microplatelets, being sufficiently thin, are expected to impart good slippage to sunscreen formulations and appear transparent when applied on the skin, offering aesthetically appealing formulations. The 2D polygonic ZnO microplatelets are expected to be advantageous for application as UFs by contributing towards obtaining a sunscreen formulation that offers high SPF and photostability while being aesthetically appealing and non-toxic.

Experimental Methodology

Materials and Chemicals

Zinc nitrate hexahydrate (98%, SRL chemicals, India), glycerol and sodium hydroxide (Sigma Aldrich, South Africa) were used as obtained from suppliers. As a reference sample for comparison purposes, the cosmetic grade ZnO was kindly supplied by AMKA Products Pty Ltd., South Africa. The ingredients used for preparing sunscreen formulations, as presented in Table 1, were used as received from suppliers. Mineral oil, glyceryl stearate/PEG-100, cetearyl alcohol, phenoxyethanol, and stearic acid were kindly provided by AMKA Products Pty Ltd., South Africa.

Synthesis of ZnO Microplatelets

ZnO microplatelets were obtained by calcinating a precursor product from a simple chemical precipitation reaction followed by an aging step. A solution of zinc nitrate hexahydrate (0.1 M, 2 L) was prepared in deionized water and magnetically stirred at 400 rpm in a suitable container. NaOH solution (1 M, 150 mL) was added dropwise to the zinc nitrate solution, under stirring, resulting in a final pH of 7 to 8. The solution was stirred for 5 minutes, and the container was then placed in a water bath at 25 °C to age the product for 72 h under stationary conditions. The residue was

Table 1. Composition of sunscreen formulations.

Ingredient	Amount (g/100 g formulation)	
wt% active	5	10
Water phase		
Water	76.2	71.2
Glycerol	5	5
Xantham gum	0.3	0.3
ZnO (active)	5	10
Oil phase		
Mineral oil	5	5
Cetearyl alcohol	4	4
Glyceryl Stearate/PEG-100	3	3
Stearic acid	1	1
Phenoxyethanol (Preservative)	0.5	0.5

recovered by centrifugation (4000 rpm, 15 min), thoroughly rinsed with deionized water, and dried in an oven at 60 °C under vacuum. The precursor product was then calcined at 300 °C for 2 h to obtain 2D ZnO microplatelets. The calcined product was ground, sieved to 75 μm, and stored in an airtight container for characterization and experimental studies.

Characterization of Structural Properties

Different techniques were employed to obtain information on the structural properties of the synthesized precursor product, ZnO microplatelets, and the ZnO reference sample for comparison purposes. Powder X-ray diffraction (PXRD) analysis was used to investigate the crystal structure of the samples. PXRD patterns were acquired for 2θ values between 5° and 90° by using a PANalytical X'Pert PRO-diffractometer (PANalytical, The Netherlands), which employs a Cu Kα radiation (λ = 1.5406 Å) source and generator voltage/tube current of 45 kV/40 mA. The surface morphologies of the samples were studied with a scanning electron microscope (SEM) (Zeiss, Germany), and images were obtained with an accelerating voltage of 3.0 kV and an aperture size of 30 μm. Samples were dispersed onto carbon tape affixed to a stub and carbon-coated before analysis. High-resolution transmission electron microscopy (HR-TEM) images of samples were obtained from a JEOL-JEM 2100 microscope (JEOL, Japan), which employs an operating voltage of 200 keV. For HR-TEM analysis, holey carbon-coated copper grid sample holders were dipped into dispersions of the samples in ethanol obtained by ultrasonication. The attenuated total reflectance Fourier transform infrared (ATR-FTIR) spectra of samples were obtained from a PerkinElmer Spectrum 100 spectrometer (PerkinElmer, USA) equipped with a Universal ATR Accessory containing a diamond/ZnSe crystal. ATR-FTIR Spectra were recorded in the 4000–400 cm^{-1} wavelength range, with the spectral resolution set at 4 cm^{-1} and the number of scans per spectrum at 16. BET surface analysis of samples was obtained using a Tristar II (Micromeritics, USA), which employs nitrogen at 77 K. The samples were degassed at 120 °C for 2 h before analysis. Thermal stability studies for samples were carried out on a TGA Q500 thermogravimetric analyzer (TA instruments, USA). The samples were heated from room temperature to 900 °C at a heating rate of 10 °C/min in an air atmosphere with a 90 mL/min flow rate.

Characterization of Optical Properties of ZnO Microplatelets

Diffuse reflectance ultraviolet-visible (DRUV-Vis) spectroscopy was used to investigate the optical properties of the precursor product, ZnO microplatelets, and ZnO reference samples. DRUV-Vis spectra were obtained in the 200–800 nm range from a PerkinElmer Lambda 750S UV-Vis spectrometer equipped with a 60 mm Spectralon® integrating sphere accessory. The DRUV-Vis spectra were used to obtain information on the UVR absorption properties of the samples and for estimation of the band gap energies through the application of the Kubelka-Munk Function.[11,12]

Investigation of Photocatalytic Activity of ZnO Microplatelets

The photocatalytic activities of the precursor product, ZnO microplatelets, and reference samples towards the photodegradation of methylene blue (MB) dye in solution were investigated under UV irradiation at two different wavelengths, λ = 254 nm (short-wave) and λ = 365 nm (long-wave). In a typical photodegradation study, a MB solution (75 mL, 5 ppm) containing 7.5 mg (10% m/v) of the dispersed sample was magnetically stirred inside a C-10 mini cabinet and irradiated with an attached UV GL-58 handheld UV lamp (6 W, 230 V~50–60 Hz). The solutions were stirred for 5 h under UVR-irradiation. Solution aliquots (3 mL) were collected at selected time intervals and replaced by adding 3 mL aliquots of deionized water to maintain the reaction mixture volume. UV-Vis analysis of the collected sample was performed on a PerkinElmer Lambda 750S UV-Vis spectrometer (Perkin Elmer, USA), with absorbances measured at the λ_{max} = 664 nm for MB. Adsorption studies were carried out in the dark (in the absence of UVR) to investigate any possible adsorption of MB on the powder ZnO samples.

In Vitro Evaluation of the Sun Protection Factor (SPF), UVA Protection Factor (UVA-PF), and Photostability of Sunscreen Formulations

For comparison, the photoprotective capacities of the ZnO microplatelets and the ZnO reference in sunscreen formulations were assessed from the in vitro determination of UVA-PFs and photostability results. O/W emulsions of a creamy formulation type containing the ZnO microplatelets at 5 wt% and 10 wt% loadings, and the ZnO reference at 10 wt% were prepared for these studies. For the preparation of the formulations, the oil and water phases (ingredients and quantities as presented in Table 1) were prepared separately and heated until the temperature reached about 70 °C. The oil phase was then transferred into the water phase under vigorous mixing. The mixture was then transferred into a suitable container and homogenized for 3 min at 6000 rpm with a T18 digital Ultra Turrax (IKA, Germany). The emulsion obtained was left to cool to room temperature, after which the preservative was added, and the final pH was adjusted to fall within the 5.5 to 6.2 range. The formulations were kept at ambient conditions for further studies.

The *in vitro* determination of the UVA-PF and photostability testing of the prepared formulations were carried out as per the procedure outlined by ISO 24443. For the tests, the formulations (1.3 mg/cm^2) were spread uniformly over the surfaces of 5 cm×5 cm poly(methylmethacrylate) (PMMA) plates. Four test plates were prepared for each sample. A blank plate coated with glycerine was also prepared similarly. The plates were then kept in the dark for 30 min before absorbance measurements at room temperature. The plates were then subjected to UV irradiation from a UV exposure source. The absorbance of UV radiation through the blank plate and the pre- and post- irradiated plates was measured using a Labsphere UV Transmittance Analyser 2000S (Labsphere, North Sutton, NH, USA). Measurements were recorded for wavelengths ranging from 290 to 400 nm at four regions of each plate, with the wavelength increment step set at 1 nm. The absorbance data obtained for pre- and post-irradiated plates were used to determine the UVA-PF, the SPF *in vivo*/UVA-PF ratio, and the critical wavelength (λ_{crit}) for each sample and to assess the photostability of samples.

In Vivo Evaluation of Skin Irritancy Potential of Sunscreen Formulations

The potential of the ZnO microplatelets to cause skin irritation was tested in accordance with the Declaration of Helsinki and the Guidelines for Good Practice in the Conduct of Clinical Trials in Human Participation in South Africa. The ethics clearance for this study was obtained from the Research and Ethics Committee at the CSIR (Reference [238]/2023), and the studies were conducted by the Photobiology Laboratory at the Sefako Makgatho Health Sciences University as per the approved protocol (MREC/H/48/2014: CR; as renewed). Twenty adult female volunteers formed the subjects in this study, five of whom had sensitive skin. The subjects all provided signed informed consent forms before the study. The

samples were tested using specially designed aluminium Finn Chambers on Scanpore® tape for occluded sites or modified Hilltop chambers for unoccluded sites. Samples and controls were applied to the inner forearm region of each subject in a randomized blinded pattern at 0 h and again after 24 h. The tested samples included an O/W emulsion containing ZnO microplatelets at 10 wt%, a sodium lauryl sulphate (SLS) solution at 1% as the positive control, and deionized water as the negative control. The sample and controls were tested as provided or prepared (neat). Observations of the test sites were made at 0-, 24-, 48-, 72- and 96 h following application of the sample/control. The test sites were covered with the chambers for the first 2×23 h, after which the chambers were removed. Color assessments were carried out in a "double-blind" manner, in 2 ways: by visual scoring and instrumental scoring, with the Minolta Cr400 Chromameter, which employs the a* value (redness), that measures color on the red/green axis. The change in a* values at each time point, when compared to the baseline, was calculated by:

$$Delta\ a^*_t = (sample\ a^*_t - sample\ a^*_0) - (baseline\ a^*_t - baseline\ a^*_0) \quad (1)$$

where a^*_t and a^*_0 are the a^* values at time t and time 0.

2. Results and Discussion

2.1. Structural Properties of ZnO Microplatelets

The XRD patterns obtained for the precursor product, ZnO microplatelets, and ZnO reference sample are presented in Figure 1a. The sharpness of the peaks indicated the crystalline nature of the precursor and ZnO microplatelets.[13] The peak positions in the XRD pattern of the precursor product were indexed to the monoclinic zinc hydroxide nitrate ($Zn_5(OH)_8(NO_3)_2.2H_2O$) lamellar phase.[13–15] The high-intensity peak at $2\theta = 9°$ corresponding to the (200) plane of the monoclinic structure, is characteristic of a layered structure with a sizeable interlayer spacing, and the corresponding d-spacing of 10 Å is consistent with that of nitrate interlayer anions.[13,14,16,17] The peak positions in the XRD patterns of the ZnO microplatelets and reference samples were indexed to the hexagonal wurtzite structure of ZnO, confirming the successful conversion of the precursor product by the calcination step.[13,17,18] The results obtained were similar to some of the findings of a study by Mrad et al.[13] that investigated the effects of varying the zinc salt precursor, reaction temperature and alkaline ratio ($[OH^-]/[Zn^{2+}]$) on ZnO synthesis via chemical precipitation in aqueous medium. Zinc hydroxide nitrate and chloride lamellar phases (precursors) were obtained at room

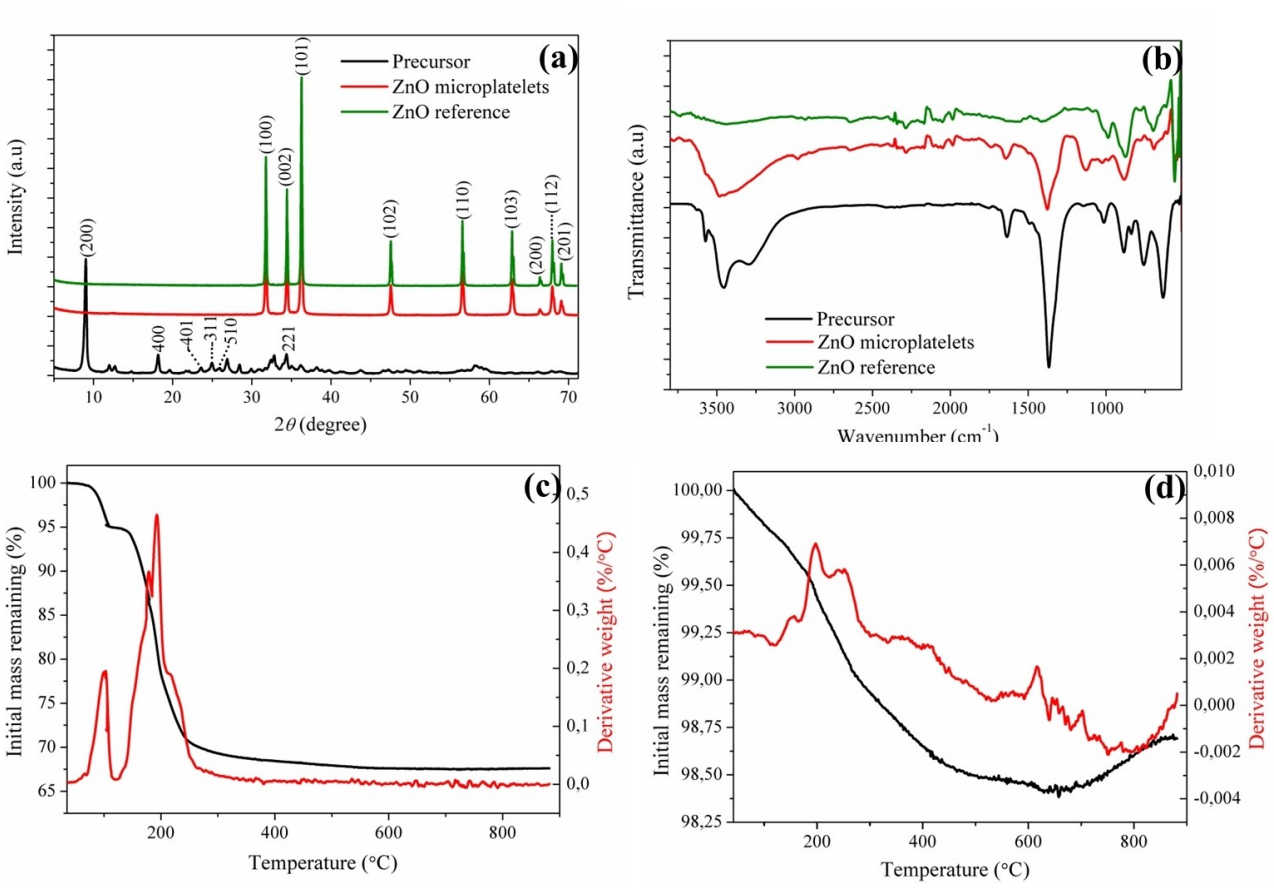

Figure 1. (a) XRD patterns, (b) ATR-FTIR spectra of precursor product, ZnO microplatelets, and ZnO reference sample, and thermograms from TGA analysis of (c) precursor product and (d) ZnO microplatelets.

temperature (20 °C) for the lower alkaline ratios of 0.5 and 1 for zinc nitrate hexahydrate and zinc chloride precursor salts, respectively. ZnO was obtained by calcinating the nitrate lamellar phase and the chloride lamellar phase in air for 2 h, at temperatures 200 °C and 350 °C and above, respectively. The study also found that ZnO was obtained at room temperature (20 °C) when the alkaline ratio was sufficiently high, above 3 for both zinc salt precursors. At the higher reaction temperature of 95 °C, ZnO was obtained with zinc nitrate hexahydrate, for alkaline ratios ranging from 1–4, and with zinc chloride, for alkaline ratios ranging from 2–4. This contrasted with our study and other studies in the literature, wherein ZnO was not directly obtained via chemical precipitation and calcination steps were required to convert the precursor to ZnO. Zareie et al.[19] prepared micro-sized ZnO flakes by calcining, at 600 °C for 4 h, a $Zn(OH)_2$ precursor obtained from a chemical precipitation reaction employing zinc sulfate pentahydrate and sodium hydroxide. Zhang et al.[20] prepared a simonkolleit ($Zn_5(OH)_8Cl_2.H_2O$) precursor by the hydrothermal treatment of a reaction mixture containing $ZnCl_2$, polyvinylpyrrolidone, an ethanol/distilled water solvent, and urea at 24 h at 90 °C. Hexagonal ZnO nanosheets were obtained by annealing the precursor at three different temperatures (300, 500 and 700 °C) for 2 h. Tseng et al.[21] prepared a zinc alkoxide precursor using a sol-gel method carried out at 160 °C with zinc acetate as the zinc ion source and glycerol as the solvent and obtained ZnO flakes by calcining the precursor at 500 °C.

The ATR-FTIR spectra obtained for the precursor product, ZnO microplatelets and ZnO reference samples are presented in Figure 1b. The spectrum for the precursor product contained bands mainly due to nitrate ions and hydroxyl functional groups present in its structure, and it corresponded well to that reported in the literature for layered zinc hydroxide nitrates.[13,14] Mrad et al.[13] and Nabipour et al.[14] assigned the bands at ca. 1367 cm^{-1}, 833 cm^{-1}, 760 cm^{-1}, and 1013 cm^{-1} to the asymmetric stretching, asymmetric and symmetric deformations, and symmetric stretching vibrations of the nitrate ion functional group, respectively, and attributed the band at 632 cm^{-1} to Zn–OH bending vibrations. The broad bands in the 3700–3000 cm^{-1} region of the spectra were attributed to O–H stretching vibrations from O–H groups or H_2O molecules, and the bands at 1640 cm^{-1} to bending vibrations of H_2O.[13,14] The spectra obtained for the ZnO microplatelets and ZnO reference sample contained bands at 558 cm^{-1}, characteristic of the ZnO stretching vibration, as reported by Raja et al.[11] Bashir et al.[22] and Balogun et al.[23] also reported peaks at 1024, 881, 696, and 606 cm^{-1} on the spectra for ZnO. The bands occurring in the 2500–2000 cm^{-1} region in the samples' spectra were attributed to vibrations arising from CO_2 molecules.[11,24]

The results obtained from the thermogravimetric analysis of the precursor product and ZnO microplatelets are shown in Figures 1c and d. The thermogram in Figure 1c showed that the degradation of the precursor involved multiple events and indicated an overall decrease in sample mass of 33% as the temperature was increased to 900 °C. Studies have attributed the mass decrease to de-hydroxylation and oxygen- and nitrogen-containing compounds released during the step-wise thermal degradation of zinc hydroxide nitrate to ZnO.[13,25,26] Moezzi et al.[26] attributed the first event, occurring between 70 and 120 °C, to the sample's water loss. The second event, between 120 and 300 °C, was attributed to the de-hydroxylation of $Zn_5(OH)_8(NO_3)_2 \cdot 2H_2O$ to $Zn_3(OH)_4(NO_3)_2$ and ZnO, between 120 and 183 °C, and the decomposition of $Zn_3(OH)_4(NO_3)_2$ to ZnO, between 183 and 300 °C.[26] Similar findings were made in studies by Mrad et al.[13] and Ramesh et al.[25] As the precursor was completely converted to ZnO by 300 °C, this temperature was selected for the calcination step of the synthesis process. The thermogram for ZnO microplatelets, shown in Figure 1d, showed a small mass decrease of 1.6% as the sample was heated to 900 °C, attributed to the removal of adsorbed water from the sample and the decomposition of hydroxide moieties by Chen et al.,[27] that confirmed the purity and stability of the sample.

The specific surface areas, pore volumes, and pore diameters, as obtained from Brunauer–Emmett–Teller (BET) and Barrett–Joyner–Halenda (BJH) analysis, were found to be 5.88 m^2/g, 0.03 cm^3/g, and 30.08 nm for the ZnO microplatelets and 3.47 m^2/g, 0.01 cm^3/g, and 13.99 nm for the ZnO reference sample, respectively. The N_2 adsorption-desorption isotherms used to calculate the specific surface areas are presented in Figure S1 (Supporting Information, SI). The adsorption isotherms for the ZnO microplatelets and reference sample were similar in shape, with low nitrogen adsorption at relative pressures up to 0.9, after which nitrogen adsorption increased sharply. The adsorption and desorption curves were closely positioned, and the narrow hysteresis loops indicated that the adsorption isotherms were of Type IV, with H1 hysteresis loops.[17] This suggested the mesoporous nature of the ZnO samples. The pore-size distribution curves in Figure S1 (SI), employed for calculating the pore volumes and diameters, confirmed that the samples were mesoporous, with pore sizes falling within the 2–50 nm range. The lower surface area of the ZnO reference sample, even though its particles were smaller than that of the ZnO microplatelets, may be due to particle aggregation. Zhang et al.[20] reported specific surface areas of 31.44, 46.95, and 9.82 m^2/g for hexagonal ZnO nanosheets obtained by annealing the $Zn_5(OH)_8Cl_2 \cdot H_2O$ precursor, synthesized via a hydrothermal method, at 300, 500 and 700 °C, respectively. Jeong et al.[28] prepared ZnO plates with a BET surface area of 11.3 m^2/g via a zinc chloride solvothermal method. For comparison, ZnO rods with a BET surface area of 10.2 m^2/g were also prepared in this study via the same method but with a different salt, zinc acetate dihydrate. The specific surface areas of commercially obtained nanometric and micrometric ZnO particles were found to be 22.0 and 4.8 m^2/g, respectively, in a study by Reinosa et al.[8] Lewicka et al.[29] reported surface areas of 9.1 to 11.2 m^2/g for ZnO extracted from different commercial sunscreens and 14.7 and 12.1 m^2/g for two different commercial ZnO references.

The SEM image in Figure 2a showed that the precursor product consisted of thin polygonal 2D microplatelets of varying sizes with smooth surfaces. Figure 2b shows that the microplatelet structure of the precursor product was maintained after the calcination process, although the surface of the

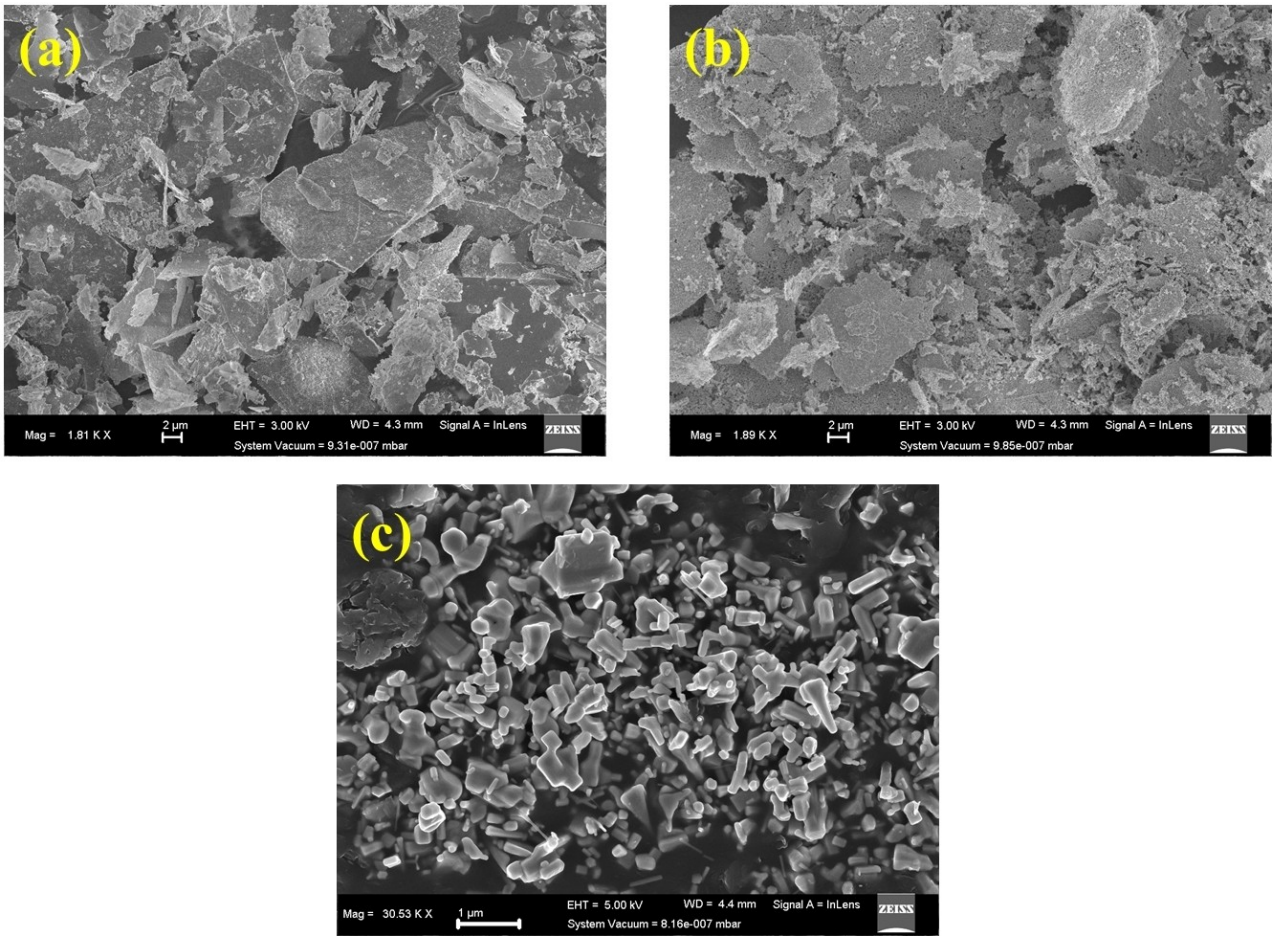

Figure 2. SEM images of (a) precursor product, (b) ZnO microplatelets, and (c) ZnO reference sample.

ZnO microplates appeared rougher and porous. Similar observations were made in other studies in the literature, where the smooth surfaces of ZnO precursors became rough after calcination and exhibited cracks and holes.[20,21,30] These structural changes were attributed to dehydration processes involved in transforming the precursor to ZnO during calcination and releasing gases such as water vapor and HNO_3.[21,26,30]

The TEM images, shown in Figure 3, confirmed the particle properties, such as the shape and dimensions of the samples studied, as obtained from SEM analysis. The lattice fringes on the HR-TEM images and selected area electron diffraction (SAED) patterns in Figure S2 (SI) confirmed the crystalline nature of the precursor product, ZnO microplatelets and ZnO reference samples, indicated by XRD analysis.[20,21,31] The TEM images

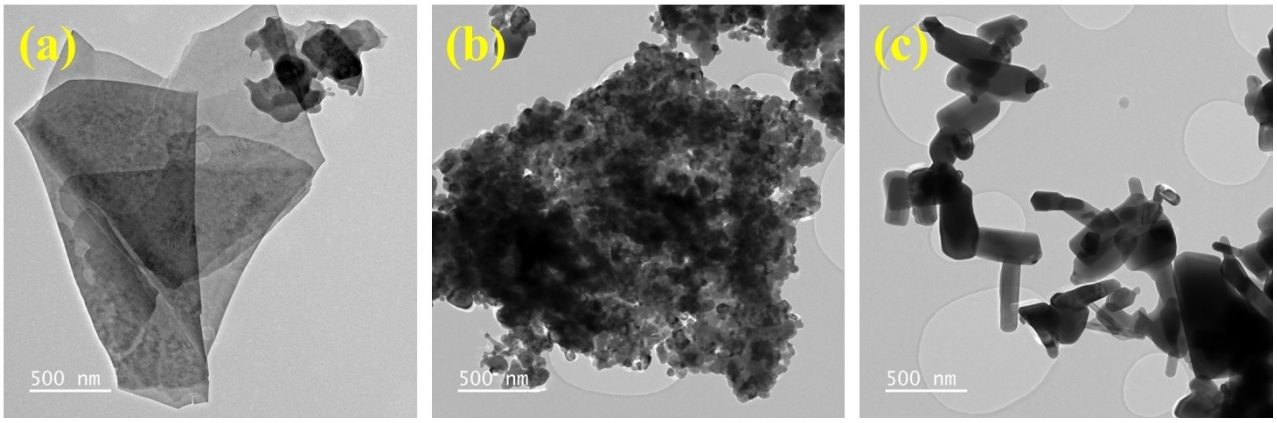

Figure 3. TEM images of (a) precursor product, (b) ZnO microplatelets, and (c) ZnO reference sample.

obtained for the precursor product (Figure 3a) showed smooth-surfaced plates, and for the ZnO microplatelets (Figure 3b) showed rough-surfaced plates that were not transparent and contained holes in their structures. The TEM image of the ZnO precursor, in Figure S3a (SI), showed that the holes of the carbon film on the Cu grid were visible through the microplates, indicating their thinness. At the same time, microplatelet thicknesses of less than 100 nm were measured on the SEM image in Figure S3b (SI). The SEM image (Figure 2c) and TEM image (Figure 3c) of the ZnO reference sample showed that it consisted of 3D particles of varying shapes and sizes with smooth surfaces, with a morphology different from that of the ZnO microplatelets. This is characteristic of commercially produced ZnO, typically used in sunscreen products.[32–34] Even though ZnO is a widely used UV filter in sunscreens, there are safety concerns related to the dermal penetration and high photoreactivity of ZnO, especially nano-sized particles.[35] Therefore, due to their larger particle sizes and platelet structure, the ZnO microplatelets are advantageous over the reference sample and nano-ZnO for use as UFs in sunscreens. Furthermore, composed of thin, platelet particles, the ZnO microplatelets are expected to impart good slippage to sunscreen formulations and offer better coverage and transparency when topically applied on the skin.[36]

Studies in the literature have indicated that the properties and morphology of ZnO particles are affected by different factors related to the synthesis reaction, such as the method type, the solvent, the pH of the medium, the temperature, the reaction duration, the type and concentration of the zinc salt precursor, precipitating agents, capping agents, and other reagents used, and the calcination conditions such as temperature and duration, amongst others.[9,10] 2D ZnO structures can be obtained by selecting an appropriate method and carefully controlling synthesis conditions such as pH, temperature, and solvent, as well as employing capping agents and surfactants.[9,10] Table 2 presents different methods and synthesis conditions reported in the literature for obtaining ZnO platelets.[19–21,30,31] When compared to this study, the methods given in Table 2 typically employed more complicated experimental setups and equipment, and higher reaction temperatures, especially the polyol and hydrothermal methods, and often required organic chemicals and solvents, capping agents, surfactants and/or substrates for obtaining ZnO plates. This study obtained ZnO microplatelets through a relatively simple method employing chemical precipitation, aging, and calcination steps. The ZnO precursor particles were synthesized via the chemical precipitation reaction, and the microplatelets formed during the aging process through the controlled aggregation of NPs. These steps employed simple starting reagents, including zinc nitrate hexahydrate salt and sodium hydroxide, and were carried out under mild conditions of temperature (25 °C) and pH (final pH between 7–8). The ZnO microplatelets were obtained by calcinating the ZnO precursor product at a relatively low temperature (300 °C) and for a short duration (2 h). Synthesis methods in Table 2 and others reported in the literature are commonly employed for obtaining ZnO of high photoreactivity, which is desired for applications such as photocatalysis and gas sensing.[20,21,28,31] The method used in this study is a convenient, scalable method that is advantageous for attaining ZnO having low photocatalytic activity, that is better suited for application as UFs in sunscreens due to human safety concerns and formulation stability issues, as discussed in a later section.

2.2. Optical Properties of ZnO Microplatelets

The DRUV-Vis spectra obtained for the precursor product, ZnO microplatelets and ZnO reference sample are presented in Figure 4a. The spectra show that the ZnO microplatelets and ZnO reference sample have low reflectance capabilities across the UV region, including the UVC, UVB, UVA-II regions and most of the UVA–I region, characteristic of ZnO.[1,4] The samples all have high reflectance in the visible region of the electromagnetic spectrum owing to their distinctive white color. The reflectance values from the DRUV-Vis spectra were converted into equivalent absorption coefficients (α) by application of the Kubelka-Munk (K–M) equation as presented below.

$$F(R) = \left(\frac{(1-R)^2}{2R}\right) \tag{2}$$

where R is the absolute reflectance value, and F(R) is proportional to α.[37] As such, the plot in Figure 4b indicates the sample's absorbance as a function of wavelength.[37] Figure 4b showed that the ZnO microplatelets had the highest UV absorbance capabilities of the samples studied, while the precursor product showed the lowest capacity for UV absorbance. This is due to the semiconducting nature of ZnO, resulting in its propensity for attenuating UVR primarily through absorption and, to a lesser extent, by reflection.[38]

The band gap energies of the samples were obtained from the Tauc plots by applying Equation (3).

$$(h\nu\alpha)^{\frac{1}{n}} = A(h\nu - E_g) \tag{3}$$

where ν is the frequency of light, h is the Plank's constant, E_g is the band gap energy, n is the order of electronic transition, and α, obtained from the Kubelka–Munk equation, is proportional to F(R).[37,39] The value of n is determined by the type of transitions that occur in a material. In the case of ZnO, direct allowed transitions occur for which an n value of $\frac{1}{2}$ is applicable.[6] The Tauc plots of the samples are presented in Figures 4c and d for the ZnO microplatelets and reference samples. The band gap energies, obtained by extrapolation of the linear portion of the Tauc plot to the x-axis, were found to be 3.2 eV for both the ZnO microplatelets and the reference sample. These values correlate well with the band gap energies of ZnO, reported in the literature. A study by Agarwal et al.,[39] wherein band gap energies of 3.26, 3.24, and 3.10 eV were reported for ZnO nanoparticles, nanosheets, and nanorods of increasing particle sizes, respectively, suggested that band gap energy decreased with an increase in crystallite size. The authors also noted that band gap energy depended on factors other than particle size,

Table 2. Comparison of the synthesis conditions reported in the literature for obtaining ZnO platelet particles.

ZnO	Method, steps	Reagents, conditions	Microscope image	Ref
Flakes	Chemical precipitation	Zinc sulfate pentahydrate Sodium hydroxide 25 °C	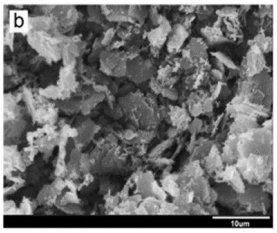	[19]
	Calcination	600 °C for 4 h		
Nanosheets	Chemical deposition on pre-modified Si substrate	Zinc acetate dihydrate Hexamine NH_3 solution	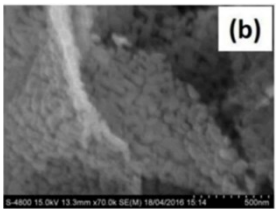	[30]
	Annealing	200 °C		
Hexagonal nanoplates	Modified-hydrothermal method on ITO[a] substrate		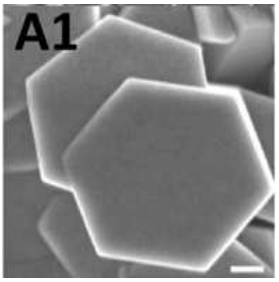	[31]
	ZnO seeding of substrate.	Zinc acetate dehydrate in ethanol		
	Annealing substrate.	350 °C in air 1 h		
	Growing NPs.	Zinc nitrate hexahydrate Hexamine		
	Aging	Aging at 4 h, 70 °C		
Nanosheets	Synthesis of hexagonal simonkolleite[b] nanosheets	One-pot hydrothermal method $ZnCl_2$, PVP[c] (Ethanol/water solvent) Autoclave 90 °C 24 h	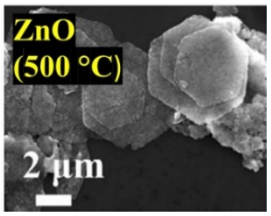	[20]
	Precursor annealed	At 300, 500, 700 °C for 2 h		
Rhombic flakes	Synthesis of precursor	Polyol method Heat up to 160 °C 1 hr under reflux Zinc acetate dihydrate Glycerol (solvent)	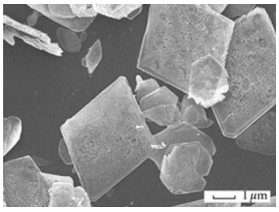	[21]
	Calcination	Up to 500 °C Keep 1 hr		
Microplatelets	Chemical precipitation	Zinc nitrate hexahydrate Sodium hydroxide 25 °C	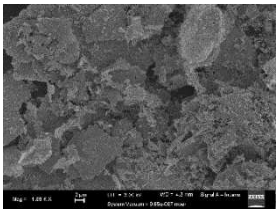	This study
	Aging	72 h, 25 °C		
	Calcination	300 °C, 2 h		

[a] Indium Tin Oxide. [b] ($Zn_5(OH)_8Cl_2{\cdot}H_2O$). [c] PVP.

such as particle morphology, the synthesis method used, and surface-related defects and/or adsorbed species. Reinosa et al.[8] found that the band gap energies of commercially obtained nanometric and micrometric ZnO particles were the same value, i.e. ~3.20 eV.

2.3. Photocatalytic Activity of ZnO Microplatelets

The propensity of ZnO to generate reactive oxygen species (ROS) such as $O_2^{-\bullet}$,$^1O_2$, and H_2O_2, and free radicals such as $^\bullet OH$, on absorption of UVR, due to its inherent photocatalytic nature

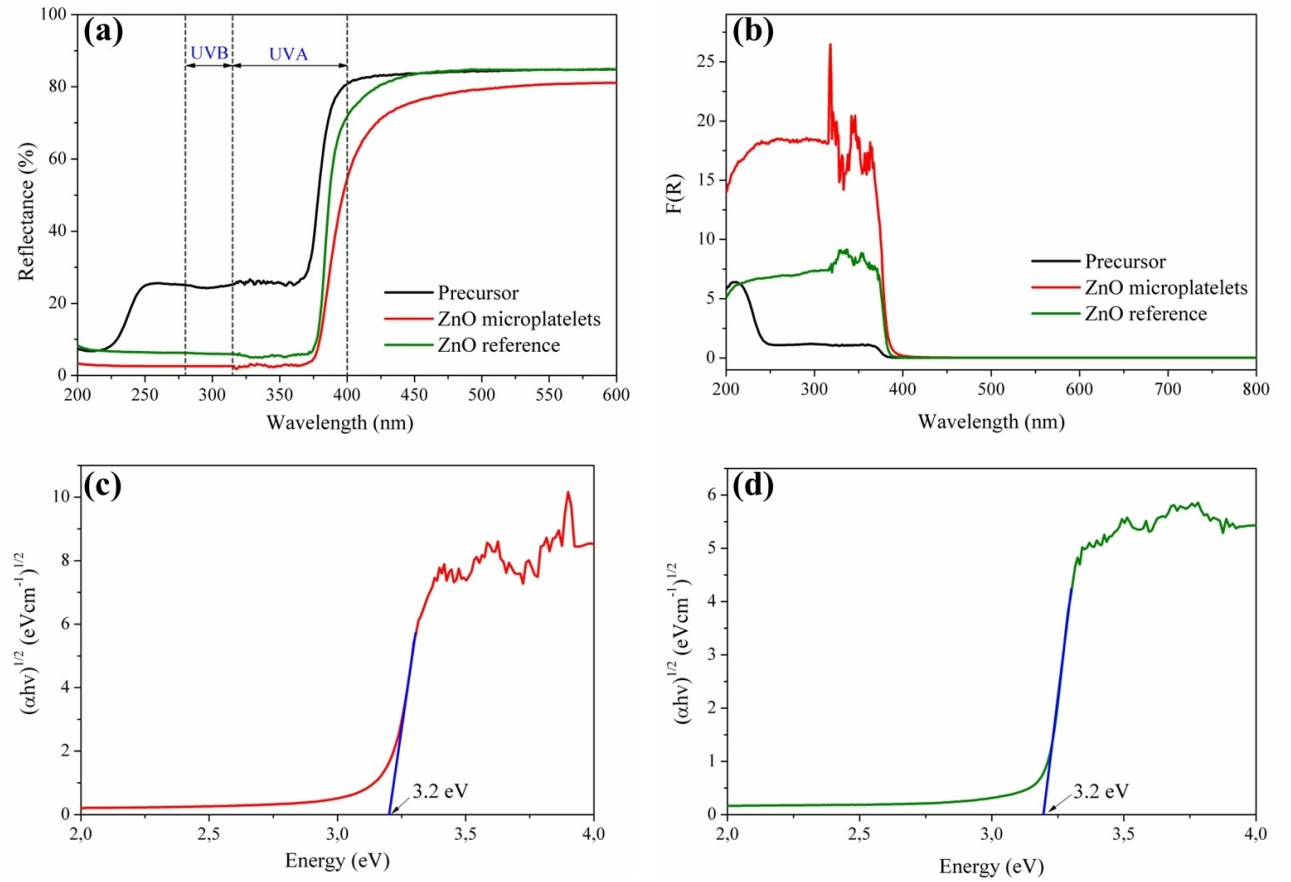

Figure 4. (a) DRUV-VIS spectra and (b) Kubelka-Munk plots obtained for the precursor product, ZnO microplatelets, ZnO reference samples, and Tauc plots for (c) ZnO microplatelets, and (d) ZnO reference sample.

has raised concerns over its use as a UV-filter in sunscreens.[1,3,5] ROS are highly reactive species that can induce oxidative stress and inflammatory responses in cells, which are linked to cytotoxic and genotoxic effects on organisms and the skin. Reactions involving ROS generated in sunscreen formulations can bring about the degradation of organic components and generate harmful organic byproducts, which may affect the formulation's appearance, stability, efficacy, and safety. Therefore, the photocatalytic activity of the ZnO microplatelets was investigated in MB dye photodegradation studies and compared to that of the precursor product and ZnO reference samples.

First, MB dye adsorption studies were carried out in the dark to determine the extent of powder samples' MB dye adsorption. Figure S4 (SI) shows the results of MB adsorption studies carried out over 5 h periods. The results suggest that the adsorption of MB by the samples was negligible over 5 h as the blank and samples show similar decreases in MB absorbance over time, associated with the dilution of the solution by the addition of deionized water to replace the sample aliquots taken. This was similar to the results of previous studies, which indicated the low adsorption capacity of ZnO for MB.[12,40–42] Also, it should be noted that the ZnO doses used for MB adsorption studies are typically higher than the low doses used for photocatalytic dye degradation studies, as in this study.[12,40–42]

After that, MB dye photodegradation studies were conducted to investigate and compare the photocatalytic properties of the ZnO precursor, ZnO microplatelets, and reference samples. In these studies, MB dye solutions in contact with the samples were irradiated for 5 h under UVR of two wavelengths, 254 nm and 365 nm. The results of the MB dye photodegradation studies carried out under UV irradiation of wavelengths 254 nm and 365 nm are presented in Figures 5a and b, respectively. Figures 5a and b show that the ZnO precursor showed no photocatalytic activity towards MB degradation under UV irradiation of both wavelengths studied, having absorbances similar to that of the blank over the 5 h period. This was expected as the ZnO precursor is not semiconducting and exhibited lower UV absorbance than the semiconducting ZnO microplatelets and the ZnO reference. MB was photodegraded by the ZnO microplatelets by 38% and 69% after 5 h under UV irradiation of 254 nm and 365 nm wavelength, respectively. In comparison, MB was photodegraded by the ZnO reference sample by 87% and 97% under UV irradiation of 254 nm and 365 nm wavelength, respectively. The ZnO microplatelets, therefore, exhibited lower photocatalytic activity towards MB photodegradation than the ZnO reference sample, which decolorized MB rapidly, with MB photodegradation occurring at a faster rate under UV irradiation of wavelength 365 nm than 254 nm for both samples.

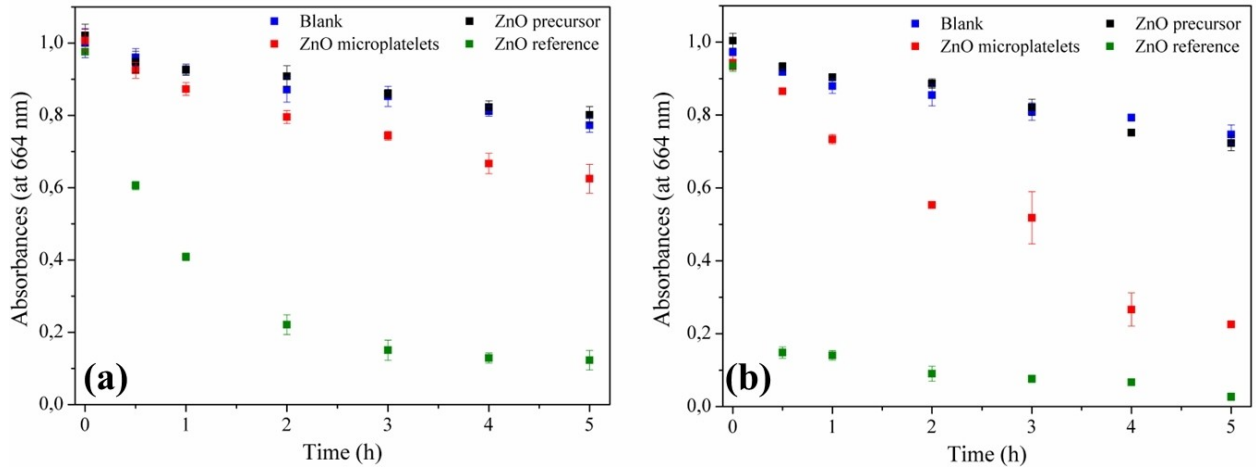

Figure 5. Photodegradation of MB dye under UV radiation of wavelength (a) 254 nm and (b) 365 nm by the precursor product, ZnO microplatelets, and ZnO reference sample over a 5 h period.

Studies in the literature have indicated the high photocatalytic activity of commercial ZnO typically used in sunscreen products.[29] Lewicka et al.[29] found that ZnO extracted from different commercial sunscreen products rapidly decolorized Congo Red dye under UVA irradiation due to the substantial levels of ROS generated. Furthermore, commercial ZnO references (Z-Cote and Z-Ald) were found to degrade Rose Bengal dye in five photodegradation cycles completely. No activity loss was observed after each cycle. Since the O_2 mediates the photodegradation of $MB^{-\bullet}$ and $^{\bullet}OH$ radicals generated on UV irradiation of ZnO, the results suggested that less ROS was generated on UV irradiation of ZnO microplatelets than on UV irradiation of the ZnO reference sample.[37,43,44] The photocatalytic activities of ZnO structures varied in studies reported in the literature. In a study by Tseng et al.,[21] the MB degradation rate was the highest for ZnO fibers, with the MB concentration decreasing by 50% after 10 min and by ~95% after 1 h. MB degradation by ZnO sheets occurred at a slower rate, similar to that of the commercial ZnO and slightly higher than that of ZnO spheres, with the MB concentrations remaining above 90% after 10 min and between ~10–20% after 1 h, for all three samples. In contrast, a study by Suwanboon et al.[45] found that hexagonal ZnO platelets degraded MB faster than rod-like ZnO particles, which was attributed to the differing planes and surface energies of the two morphologies. The photocatalytic activity of ZnO nanoplatelets towards the photodegradation of eosin B was found to be higher than that of ZnO nanorods and comparable with that of commercial titania particles (Degussa P25) in a study by Ye et al.[46] The authors attributed the higher photocatalytic efficiency of the ZnO nanoplatelets than the nanorods to the thin structure and higher surface-to-volume ratio of the nanoplates and the presence of polar surface planes in its structure, which may have adsorbed the organic dye better than non-polar-planes-present-in the nanorods. However, it must be noted that the dimensions (particle size and thickness) and shapes of the ZnO platelets varied significantly in the studies compared above.

The photocatalytic activity of ZnO depends on many factors, such as particle size distribution, surface area, crystallinity, morphology, band gap energy, crystal facets, and bulk and surface defects.[37,47,48] Battistin et al.[49] observed that the photocatalytic activity of ZnO samples towards the photodegradation of Acid Blue 9 dye was dependent on particle size and surface area, with the ZnO sample having the highest surface area and the most significant proportion of nanometric particles exhibiting the highest photoactivity. However, even though a high surface area is advantageous, implying the high availability of active sites, studies have indicated that a high surface area does not always translate to a high photocatalytic activity.[37,47] In this study, the differing photocatalytic activities of the ZnO microplatelets and the ZnO reference sample could not be explained regarding their band gap energies or specific surface areas due to their same or similar values, respectively. Here, the photocatalytic activities of the ZnO microplatelets and the ZnO reference sample can be attributed to their crystallinity, morphology, and microstructural properties. Due to its higher crystallinity than that of ZnO microplatelets, as observed from the XRD spectra in Figure 1a, the ZnO reference sample contains fewer bulk defects and, therefore, a higher concentration of surface-to-bulk defects, which translates to better separation efficiency of photogenerated e^-/h^+ pairs and higher photocatalytic activity.[47,48] Surface defects on semiconducting metal oxides such as ZnO act as charge carrier traps and adsorption sites, thus facilitating the transfer of charge carriers to species adsorbed on the surface and preventing the recombination of e^-/h^+ pairs. Bulk defects, on the other hand, can serve as sites for recombining photogenerated e^-/h^+ pairs and thus reduce photocatalytic activity. The ZnO microplatelets have a lower concentration of surface-to-bulk defects due to their lower crystallinity and, therefore, lower photocatalytic activity. The synthesis method used in this study for obtaining the ZnO microplatelets may have resulted in a structure with a higher proportion of bulk defects than that of ZnO obtained from other synthesis methods, which resulted in their lower photocatalytic activity that renders ZnO microplatelets advanta-

geous over the commercial ZnO reference for application as UFs in sunscreens. Due to its good UVR attenuation capacity, lower photocatalytic activity and platelet structure, the ZnO microplatelets are also ideal for use in other applications, such as in protective coatings and textiles, where ZnO is typically employed for its UV-shielding and antimicrobial properties.[50,51] In these applications, ZnO of high photocatalytic activity is undesirable due to its potential to cause adverse effects to material integrity and the dyes' photodegradation.[50,51]

2.4. SPF and UVA-PF of Sunscreen Formulations

Sunscreen formulations containing the ZnO microplatelets and the ZnO reference sample were prepared to investigate their performance as UFs towards photoprotection. The results obtained from *in vitro* UVA-PF and SPF testing of the formulations carried out as per the testing procedure outlined by ISO 24443, with a Labsphere UV Transmittance Analyser 2000S, are given in Table 3. The formulation containing ZnO microplatelets at 5 wt% had the highest average SPF value, 11.56, and the lowest average UVA-PF value, 5.07, of the formulations tested. The formulations containing ZnO microplatelets and the ZnO reference, at 10 wt%, had similar average SPF values of 6.15 and 6.33 and average UVA-PF values of 9.25 and 8.53, respectively. Sunscreen formulations with a mean λ_{crit} of 370 nm or higher can be classified as broad-spectrum based on the SANS 1557 standard.[52] In addition, for products to be classified as offering UVA protection, the sunscreen formulation must have a UVA balance of 33% or above.[52] Therefore, all the sunscreen formulations tested met the criteria to be categorized as broad-spectrum products offering UVA protection.

Porrawatkul et al.[53] reported SPF and UVA-PF values, determined *in vitro*, of 10.10 and 7.83, respectively, for a sunscreen formulation containing ZnO NPs of sizes ranging from 63 nm–69 nm, prepared via a microwave method employing plant extracts of *Averrhoa carambola*. The SPF of sunscreen formulations containing commercially obtained ZnO powder, comprising mainly ZnO nanorods, at 5 and 10 wt%, were found to be 29.5 and 36.1 from *in vitro* studies, respectively, by Zaki et al.[54] Khalil et al.[55] found a sunscreen formulation containing 20 wt% ZnO powder, with a specific surface area of 20 m^2/g and particle sizes of 20 to 50 nm, with an SPF of 10 from the *in vitro* studies. The SPF values of two sunscreen formulations containing different commercial references, also at 20 wt%, were 4 and 11, determined for comparison purposes. All three sunscreen formulations tested by Khalil et al.[55] had λ_{crit} values above 370 nm. Therefore, the SPF of the sunscreen formulation containing ZnO microplatelets compares well to SPF values reported in the literature for formulations containing different ZnO UFs. Furthermore, the ZnO microplatelets obtained in this study have additional advantages of being microsized in two dimensions and having lower photocatalytic activity than commercial ZnO microparticles and NPs.

2.5. Photostability of Sunscreen Formulations

The *in vitro* determination of the UVA-PF and SPF values of the sunscreen formulations containing ZnO microplatelets and reference samples were carried out pre- and post-irradiation to examine the photostability of the sunscreens and the results are presented in Table 4 and Figure S5 (SI). The SPF value and UV absorbances of the sunscreen formulation containing 5 wt% ZnO microplatelets were lower post-irradiation. However, this formulation's λ^{crit} and UVA/UVB ratio values were still maintained after irradiation. The pre- and post-irradiation UV absorbances and other tested parameters of the sunscreen formulations containing 10 wt% ZnO microplatelets and the ZnO reference sample were similar in value, indicating these sunscreen formulations were photostable and of higher photostability than the formulation containing 5 wt% ZnO microplatelets.

The sunscreen formulations containing ZnO microplatelets are expected to be more stable over time than those containing the ZnO reference sample due to the lower photocatalytic activity of the ZnO microplatelets, resulting in the generation of lower concentrations of free radicals and ROS on UV exposure, as these species are associated with the degradation of organic UFs and other organic components.[1,7] Battistin et al.[49] found that commercial ZnO degraded two organic UFs, Diethylamino Hydroxybenzoyl Hexyl Benzoate (DHHB), by 3.85% and 34.77%, and Ethylhexyl Triazone (EHT), by 0.14% and 14.08%, in ethanol and water mediums, respectively. DHHB, EHT and ZnO are considered "reef-safe" UFs and could be combined in sunscreen formulations. The higher degradation of DHHB was attributed to its hydrophilic nature, which enabled greater interaction with $^{\bullet}OH$, which occurred to a lesser extent in the case of EHT due to its lipophilic nature. Ginzburg et al.[7] reported on the photodegradation of organic UFs on UVR irradiation of five different formulations, comprised of mixtures of common organic UFs, with added ZnO, and a corresponding decrease in their UVA protection. The photodegradation of organic UFs did not occur on UV irradiation of the five base sunscreen formulations, with no ZnO present. The ZnO microplatelets prepared in this study, having lower photoactivity, are also advantageous over com-

Table 3. Results from the *in vitro* determination of the UVA-PFs of sunscreen formulations containing ZnO microplatelets and reference sample.

Sample	% active	SPF (Mean)	UVA-PF (Pre-Irradiation)	UVA-PF	In vivo SPF/ UVA-PF	UVA balance	λ_{crit} (nm)
ZnO microplatelets	5%	11.56 ± 0.80	7.24 ± 0.01	5.07 ± 0.33	1.58	58%	385.75
	10%	6.15 ± 0.26	7.89 ± 0.04	9.25 ± 0.58	0.86	118%	385.19
ZnO reference	10%	6.33 ± 0.32	8.49 ± 0.01	8.53 ± 0.39	0.94	108%	386.00

Table 4. Pre- and post-irradiation results from the *in vitro* determination of the UVA-PFs of sunscreen formulations containing ZnO microplatelets and reference samples.

Sample	% active	In vitro SPF[a]	T[a] (UVA) (%)	T[a] (UVB) (%)	λ_{crit} (nm)	UVA/UVB ratio[b]
Pre-irradiation						
ZnO microplatelets	5	12.13 ± 0.73	11.78 ± 0.71	8.88 ± 0.67	385.44 ± 0.13	0.898
	10	6.31 ± 0.28	18.99 ± 0.72	16.68 ± 0.74	385.50 ± 0.00	0.940
ZnO reference	10	6.48 ± 0.36	17.18 ± 0.72	16.23 ± 0.75	386.00 ± 0.00	0.981
Post-irradiation						
ZnO microplatelets	5	7.05 ± 0.28	17.01 ± 0.73	14.46 ± 0.72	385.75 ± 0.00	0.929
	10	7.45 ± 0.38	17.46 ± 0.9	15.20 ± 0.88	385.19 ± 0.13	0.940
ZnO reference	10	6.48 ± 0.13	17.20 ± 0.44	16.14 ± 0.43	386.00 ± 0.00	0.979

[a] Spectral transmission. [b] The ratio of the area under the curve corresponding to UVB region (between 290–320 nm) to the area under the curve corresponding to the UVA region (between 320–400 nm).

mercial ZnO for use in combination sunscreens, which incorporate both inorganic and organic UFs. Combining UFs is an often-used method in industry for achieving broad-spectrum, high-SPF sunscreen formulations.[3,4]

2.6. Skin Irritancy Potential of Sunscreen Formulations

The potential of the ZnO microplatelets to cause skin irritancy was investigated in an *in vivo* study. The skin irritancy study was completed by nineteen of the twenty adult female subjects who volunteered for the tests. The circumstances leading to the incompletion of the study by one of the volunteers were unrelated to the study. The sample tested was an O/W emulsion containing ZnO microplatelets at 10 wt%, with sodium lauryl sulphate (SLS) at 1% used as a positive control and deionized water used as a negative control. The erythemal reactions on the subjects' skin to the applied sample and controls were assessed visually and with a chromameter after 24 h time intervals, up to 96 h after application. The results obtained from the visual assessment in Figure 6a showed that the positive control was irritating to the skin, with scores that typically increased with time. The negative control and the sample tested, with low scores at each time interval, were non-irritating. The irritancy values (calculated by the sum of the mean visual score and one standard deviation (SD) of the mean visual score), shown as dashed lines in Figure 6a, indicated that the positive control was an irritant after 48, 72, and 96 h of application, where the scores were above the irritancy limit (1.5). The irritancy values of the sample were lower than the irritancy limit and lower than that of the negative control for all time intervals, indicating that the sample was non-irritant. The maximum irritancy values obtained for the sample, positive control, and negative control and their corresponding time points are summarized in Figure 6c. The chromameter results in Figure 6b had similar patterns to the visually obtained values, thus supporting the visually determined data. The low delta a* values obtained for the sample indicated its non-irritant nature, while the high delta a* values obtained for the positive control indicated it was irritating to the skin. The results obtained here were as expected as inorganic UFs such as ZnO and TiO_2 were found to be non-irritating to skin in different studies and are generally favoured by sunscreen users with sensitive and compromised skin over organic UFs, some of which are known to cause skin allergies and sensitization.[4,56]

3. Conclusions

This study focused on the synthesis and characterization of 2D polygonic ZnO microplatelets and the evaluation of their performance for potential application as UFs in sunscreen products. ZnO microplatelets were prepared via a relatively simple synthesis method, which entailed the calcination of a precursor obtained by aging the product of a chemical precipitation reaction. SEM and TEM imaging confirmed the formation of thin polygonal microplatelets with rough surfaces. XRD analysis confirmed that the microplatelets were composed of highly crystalline ZnO of hexagonal wurtzite structure. Analysis of the DRUV-Vis spectra showed that the ZnO microplatelets exhibited low reflectance and high absorbance across the UV region, comparable to that of a commercial ZnO reference sample. The band gap energy of the ZnO microplatelets, obtained from the Tauc plot, was the same as that of the ZnO reference sample (3.2 eV). The BET-specific surface area of the ZnO microplatelets (5.88 m^2/g) was slightly higher than that of the ZnO reference sample (3.47 m^2/g). The ZnO microplatelets showed significantly lower photocatalytic activity than the ZnO reference sample in MB photodegradation studies carried out under UV irradiation of two different wavelengths (254 nm and 365 nm). The lower photocatalytic activity of the ZnO microplatelets was related to the lower concentration of surface-to-bulk defects in its structure due to its lower crystallinity than that of the ZnO reference sample, with the synthesis procedure used attributed to creating bulk defects in its structure. A sunscreen formulation containing ZnO microplatelets at 10 wt% had similar average SPF values and average UVA-PF values (6.15 and 9.25) to a formulation containing the ZnO reference sample at 10 wt% (6.33 and 8.53), respectively, and with λ_{crit} values above 370 nm, both formulations met the

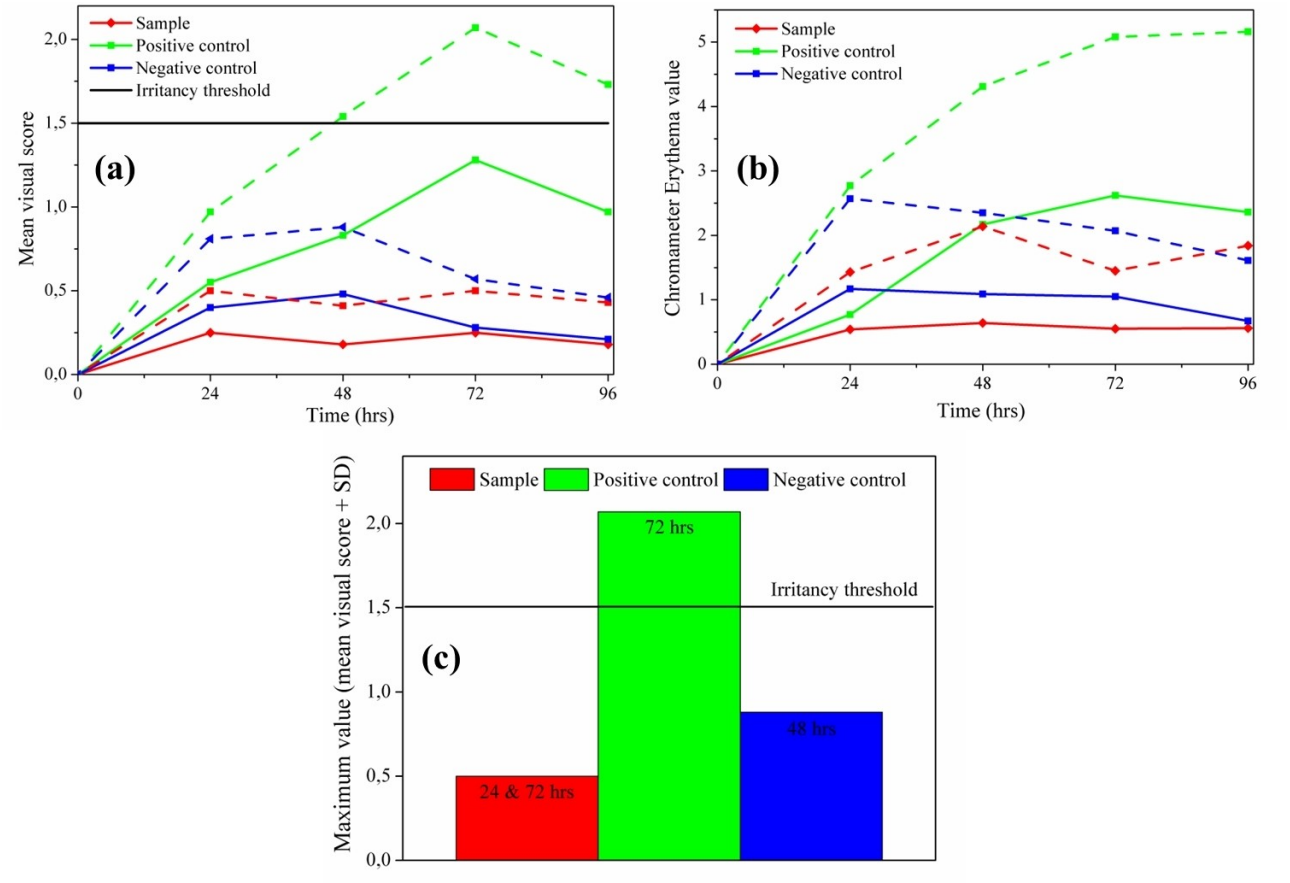

Figure 6. Mean erythema values measured: (a) visually and (b) using a chromameter for 96 h at 24 h intervals after application, and (c) Bar graph showing the maximum visual erythema values (mean + SD) of the sample, positive control and negative control.

requirements to be categorized as broad-spectrum sunscreens offering UVA protection. The pre-and post-irradiation UV absorbances and other tested parameters of the sunscreen formulation containing ZnO microplatelets at 10 wt% did not differ significantly, which indicated the photostability of the sunscreen formulation, similar to that of the ZnO reference sample-containing formulation. The formulation containing ZnO microplatelets at 10 wt% was classified as a non-irritant in an *in vivo* skin irritancy study. Therefore, ZnO microplatelets exhibiting high UVR absorbance capacity and good performance in sunscreen formulations, on par with that of commercial ZnO, were successfully obtained in this study. Furthermore, the ZnO microplatelets displayed lower photocatalytic activity than commercial ZnO and are potentially more advantageous for use as UFs in sunscreens.

4. Supporting Information Summary

Additional supporting information can be found online in the Supporting Information section at the end of this article.

Acknowledgements

The authors would like to acknowledge the Department of Science and Innovation (C6E0085), Council for Scientific and Industrial Research (C1E0080), and the University of Johannesburg, South Africa, for their financial support. The authors also thank AMKA Products (Pty) Ltd. (South Africa) for supplying the ingredients for formulation preparation. The CeNAM characterization facility is also acknowledged for supporting this research project.

Conflict of Interests

The authors declare no conflict of interest.

Data Availability Statement

The data that support the findings of this study are available from the corresponding author upon reasonable request.

Keywords: Inorganic UV filters · 2D Zinc oxide microplatelets · Photoprotection · UVR-absorption · Photocatalytic activity · Semiconductors · Sun protection factor

[1] N. Serpone, *Photochem. Photobiol. Sci.* **2021**, *20*, 189–244.
[2] S. L. Schneider, H. W. Lim, *Photodermatol. Photoimmunol. Photomed.* **2019**, *35*, 442–446.
[3] J. P. Paiva, R. R. Diniz, A. C. Leitão, L. M. Cabral, R. S. Fortunato, B. A. M. C. Santos, M. de Pádula, *Crit. Rev. Toxicol.* **2020**, *50*, 707–723.
[4] E. B. Manaia, R. C. K. Kaminski, M. A. Corrêa, L. A. Chiavacci, *Braz. J. Pharm. Sci.* **2013**, *49*, 201–209.
[5] T. G. Smijs, S. Pavel, *Nanotechnol., Sci. Appl.* **2011**, *4*, 95–112.
[6] J. J. Reinosa, C. M. Á. Docio, V. Z. Ramírez, J. F. F. Lozano, *Ceram. Int.* **2018**, *44*, 2827–2834.
[7] A. L. Ginzburg, R. S. Blackburn, C. Santillan, L. Truong, R. L. Tanguay, J. E. Hutchison, *Photochem. Photobiol. Sci.* **2021**, *20*, 1273–1285.
[8] J. J. Reinosa, P. Leret, C. M. Álvarez-Docio, A. Del Campo, J. F. Fernández, *Bol. Soc. Esp. Ceram. Vidrio.* **2016**, *55*, 55–62.
[9] S. G. Leonardi, *Chemosensors.* **2017**, *5*, 17.
[10] E. Y. Shaba, J. O. Jacob, J. O. Tijani, M. A. T. Suleiman, *Appl. Water Sci.* **2021**, *11*, 48.
[11] K. Raja, P. S. Ramesh, D. Geetha, *Spectrochim. Acta Part A* **2014**, *131*, 183–188.
[12] Y. Hendrix, E. Rauwel, K. Nagpal, R. Haddad, E. Estephan, C. Boissière, P. Rauwel, *Nanomaterials* **2023**, *13*, 1998.
[13] M. Mrad, B. Chouchene, T. B. Chaabane, *S. Afr. J. Chem.* **2018**, *71*, 103–110.
[14] H. Nabipour, M. H. Sadr, N. Thomas, *J. Exp. Nanosci.* **2015**, *10*, 1269–1284.
[15] Q. Li, S. Guo, Y. Cheng, X. Chen, Z. Tang, *Mater. Des.* **2022**, *224*, 111296.
[16] B. Saifullah, P. Arulselvan, M. E. El Zowalaty, S. Fakurazi, T. J. Webster, B. Geilich, M. Z. Hussein, *Sci. World J.* **2014**, *2014*, 401460.
[17] S. H. H. Al Ali, M. Al-Qubaisi, M. Z. Hussein, Z. Zainal, M. N. Hakim, *Int. J. Nanomed.* **2011**, *6*, 3099–3111.
[18] L. Motelica, B. S. Vasile, A. Ficai, A. V. Surdu, D. Ficai, O. C. Oprea, E. Andronescu, G. Mustăţea, E. L. Ungureanu, A. A. Dobre, *Pharmaceutica* **2023**, *15*, 2740.
[19] M. Zareie, A. Gholami, M. Bahrami, A. H. Rezaei, M. H. Keshavarz, *Mater. Lett.* **2013**, *91*, 255–257.
[20] Y. Zhang, C. Liu, F. Gong, B. Jiu, F. Li, *Mater. Lett.* **2017**, *186*, 7–11.
[21] Y. K. Tseng, M. H. Chuang, Y. C. Chen, C. H. Wu, *J. Nanobiotechnol.* **2012**, *2012*, 712850.
[22] S. Bashir, M. S. Awan, M. A. Farrukh, R. Naidu, S. A. Khan, N. Rafique, S. Ali, I. Hayat, I. Hussain, M. Z. Khan, *Int. J. Nanomed.* **2022**, *17*, 4073–4085.
[23] S. W. Balogun, O. O. James, Y. K. Sanusi, O. H. Olayinka, *SN Appl. Sci.* **2020**, *2*, 504.
[24] D. Nipane, S. R. Thakare, N. T. Khati, *J. Catal.* **2013**, *2013*, 940345.
[25] T. N. Ramesh, T. L. Madhu, *Int. J. Inorg. Chem.* **2015**, *2015*, 536470.
[26] A. Moezzi, P. S. Lee, A. M. McDonagh, M. B. Cortie, *J. Solid State Chem.* **2020**, *286*, 121311.
[27] W. Chen, X. Liu, Y. Liu, H. Il Kim, *Colloid Polym. Sci.* **2010**, *288*, 1393–1399.
[28] H. W. Jeong, S. Y. Choi, S. H. Hong, S. K. Lim, D. S. Han, A. Abdel-Wahab, H. Park, *J. Phys. Chem. C.* **2014**, *118*, 21331–21338.
[29] Z. A. Lewicka, W. W. Yu, B. L. Oliva, E. Q. Contreras, V. L. Colvin, *J. Photochem. Photobiol. A* **2013**, *263*, 24–33.
[30] P. K. Baviskar, G. P. Patil, V. S. Bagal, B. R. Sankapal, P. G. Chavan, *J. Nanostruct.* **2018**, *8*, 217–224.
[31] S. T. Tan, A. A. Umar, M. M. Salleh, *J. Alloys Compd.* **2015**, *650*, 299–304.
[32] P. J. Lu, S. W. Fang, W. L. Cheng, S. C. Huang, M. C. Huang, H. F. Cheng, *J. Food Drug Anal.* **2018**, *26*, 1192–1200.
[33] P. J. Lu, S. C. Huang, Y. P. Chen, L. C. Chiueh, D. Y. C. Shih, *J. Food Drug Anal.* **2015**, *23*, 587–594.
[34] Z. A. Lewicka, A. F. Benedetto, D. N. Benoit, W. W. Yu, J. D. Fortner, V. L. Colvin, *J. Nanopart. Res.* **2011**, *13*, 3607–3617.
[35] S. M. N. Mohsin, M. Z. Hussein, S. H. Sarijo, S. Fakurazi, P. Arulselvan, T. Y. Y. Hin, *Chem. Cent. J.* **2013**, *7*, 26.
[36] U. Ulusoy, *Minerals* **2023**, *13*, 91.
[37] S. H. Ferreira, M. Morais, D. Nunes, M. J. Oliveira, A. Rovisco, A. Pimentel, H. Águas, E. Fortunato, R. Martins, *Materials (Basel)* **2021**, *14*, 2385.
[38] C. Cole, T. Shyr, H. Ou-Yang, *Photodermatol. Photoimmunol. Photomed.* **2016**, *32*, 5–10.
[39] S. Agarwal, L. K. Jangir, K. S. Rathore, M. Kumar, K. Awasthi, *Appl. Phys. A Mater. Sci. Process.* **2019**, *125*, 553.
[40] F. Zhang, J. Lan, Y. Yang, T. Wei, R. Tan, W. Song, *J. Nanopart. Res.* **2013**, *15*, 2034.
[41] S. Ahmadi, C. A. Igwegbe, *Sigma. J. Eng. Nat. Sci.* **2020**, *38*, 289–303.
[42] T. M. Elmorsi, M. H. Elsayed, M. F. Bakr, *Can. J. Chem.* **2017**, *95*, 590–600.
[43] I. Khan, K. Saeed, I. Zekker, B. Zhang, A. H. Hendi, A. Ahmad, S. Ahmad, N. Zada, H. Ahmad, L. A. Shah, T. Shah, I. Khan, *Water* **2022**, *14*, 242.
[44] D. Zhang, F. Dai, P. Zhang, Z. An, Y. Zhao, L. Chen, *Mater. Sci. Eng. C* **2019**, *96*, 684–692.
[45] S. Suwanboon, S. Klubnuan, N. Jantha, P. Amornpitoksuk, P. Bangrak, *Mater. Lett.* **2014**, *115*, 275–278.
[46] C. Ye, Y. Bando, G. Shen, D. Golberg, *J. Phys. Chem. B.* **2006**, *110*, 15146–15151.
[47] A. K. Mourya, R. P. Singh, T. Kumar, A. S. Talmale, G. S. Gaikwad, A. V. Wankhade, *Inorg. Chem. Commun.* **2023**, *154*, 110850.
[48] D. Liu, Y. Lv, M. Zhang, Y. Liu, Y. Zhu, R. Zong, Y. Zhu, *J. Mater. Chem. Part A.* **2014**, *2*, 15377–15388.
[49] M. Battistin, P. Pascalicchio, B. Tabaro, D. Hasa, A. Bonetto, S. Manfredini, A. Baldisserotto, A. Scarso, P. Ziosi, A. Brunetta, F. Brunetta, S. Vertuani, *Antioxidants (Basel)* **2022**, *11*, 2209.
[50] L. Motelica, B. S. Vasile, A. Ficai, A. V. Surdu, D. Ficai, O. C. Oprea, E. Andronescu, D. C. Jinga, A. M. Holdan, *Pharmaceutica* **2022**, *14*, 2842.
[51] L. Motelica, O. C. Oprea, B. S. Vasile, A. Ficai, D. Ficai, E. Andronescu, A. M. Holban, *Int. J. Mol. Sci.* **2023**, *24*, 5677.
[52] D. Twilley, D. Moodley, H. Rolfes, I. Moodley, L. J. McGaw, B. Madikizela, B. Summers, L. Raaff, M. Lategan, L. Kgatuke, E. C. Mabena, N. Lall, *S. Afr. J. Bot.* **2021**, *137*, 171–182.
[53] P. Porrawatkul, P. Nuengmatcha, A. Kuyyogsuy, R. Pimsen, P. Rattanaburi, *J. Photochem. Photobiol. Part B.* **2023**, *240*, 112668.
[54] N. A. A. Zaki, S. Mahmud, A. F. Omar, *J. Phys. Conf. Ser.* **2018**, *1083*, 012012.
[55] T. Khalil, M. Köhler, K. Wegner, M. Ommer, *SOFW J.* **2023**, *149*, 4–10.
[56] M. Vujovic, E. Kostic, *J. Cosmet. Sci.* **2019**, *70*, 223–234.

Manuscript received: June 20, 2024